Random sampling remap for compressible two-phase flows

Mathieu Bachmann, Philippe Helluy, Jonathan Jung, Hélène Mathis, Siegfried Müller

RANDOM SAMPLING REMAP FOR COMPRESSIBLE TWO-PHASE FLOWS

M. BACHMANN, P. HELLUY, H. MATHIS AND S. MÜLLER

Abstract. In this paper, we address the problem of solving accurately gas-liquid compressible flows, without pressure oscillations at the gas-liquid interface. We introduce a new Lagrange-projection scheme based on a random sampling technique introduced by Chalons and Goatin in [CG07]. We compare it to a Ghost Fluid approach introduced in [WLK06] and [MBKKH09]. Despite the non-conservative feature of the schemes, we observe the numerical convergence towards the relevant weak solution, for shock-contact interaction test cases. Finally, we apply the new scheme to the computation of the oscillations of a spherical air bubble inside water.

Introduction

The bad precision of conservative Godunov schemes applied to two-fluid flows is a subject that has been studied now for more than twenty years (see [Abg88, Kar94, SA99a, BHR03, MBKKH09] and included references). This bad precision implies perturbations on the pressure profiles, that are often called the "pressure oscillations" phenomenon.

For the moment, it has not been possible to design a simple conservative scheme that preserves the constant velocity-pressure states. This property, which amounts to preserving the contact discontinuities in one-dimensional flows, seems to be mandatory for obtaining reliable schemes. Thus, many authors have proposed modified Godunov schemes in order to achieve this property. Karni, in [Kar94] proposes to solve the pressure evolution equation instead of the mass fraction evolution equation at the interface. Abgrall and Saurel [Abg88, SA99a] propose to solve the mass fraction equation in a non-conservative way in order to recover the preservation of constant velocity-pressure states (SA approach). Fedkiw and collaborators [FAMO99] introduce the Ghost Fluid (GF) method: at the interface, they propose to introduce two virtual fluids in order to construct a scheme that only requires a one-fluid Riemann solver. The GF method has been improved in many works. We will concentrate here in one variant, the Real Ghost Fluid Method (RGFM) [WLK06, MBKKH09]. It is not possible to give a comprehensive survey of this field, but many other attempts have been proposed: changing the two-fluid model to a more general one [SA99b, WK05, KL10], using a Lagrangian approach at the interface [HMM08], *etc.*

A common feature of all the above-mentioned approaches is that the schemes are generally non-conservative. It is possible to construct very exotic schemes that are conservative but they are then very complicated and can be used only for academic test cases [HMM08]. A natural question arises, which is whether these schemes

Key words and phrases. Finite volume, Godunov scheme, Ghost fluid method, lagrange-projection, Glimm scheme, gas bubble oscillations.

converge, or not, towards the relevant solution of the initial two-fluid models. Indeed, generally, non-conservative schemes converge towards wrong solutions. It is a purely non-linear behavior [HL94], which is still not yet well understood because a non-conservative Lax-Wendroff theory does not exist (for a recent work on this aspect, see [AK10]). Here, the situation is rather subtle because the non-conservation of the schemes is generally located at the contact discontinuity, which is a linearly degenerated field. When all the discontinuous waves (shocks and contacts) are well separated, it is thus not a full paradox to observe convergence towards the good solution. However, in case of complicated non-linear interactions, when all the waves are mixed, it is difficult to understand why the non-conservative approach leads to well converging schemes. For one-dimensional problems, wave mixing occur in very simple situations: at the initial time of a Riemann problem, for instance, or when a shock wave is sent over a moving interface.

Our first objective in this paper is to provide a new non-conservative scheme for solving two-fluid flows. Our approach is an adaptation of previous works of Goatin, Chalons and Coquel [CG07, CC08] on Lagrange-projection schemes. The idea is to use a projection step based on random sampling techniques, very similar to the Glimm scheme method. The classical Glimm scheme [Gl65] implies an exact Riemann solver. Here, because the random sampling is only performed in the projection step, it is possible to rely on approximate Riemann solvers in the Lagrange step. We will see that in presence of strong shocks, our approach has to be adapted, in order to avoid oscillations and non-convergence: we simply propose to perform the random sampling strategy only at the two fluids interface. As for other schemes, our random sampling projection scheme is not conservative. Let us recall that the Glimm scheme is not conservative too, but possesses statistically conservation properties [Gl65]. We hope that such properties still hold for our sampling projection scheme.

Our second objective is to perform a numerical convergence study for several classical non-conservative schemes for two-fluid flows, and compare them to our new scheme. We will observe, surprisingly, that the numerical solutions seem to converge towards the good weak solutions. According to our previous considerations, this behavior is absolutely not obvious. Finally, we compare our new scheme to the RGFM in a more complex configuration. We present a hard test case consisting in computing the oscillations of a spherical gas bubble in a compressible liquid. We present the results obtained with the RGFM and the random projection scheme.

1. The two-fluid model

In this paper, we investigate the numerical resolution of the Euler system for a compressible two-fluid mixture. The density of the mixture is ρ, the velocity is u and the internal energy is e. We denote by E the total energy defined by $E = e + u^2/2$. The pressure is noted p. For simplicity, but without loss a generality, we only consider one-dimensional flows. The unknowns depend on the spatial position x and of the time t. The PDE system is made of mass, momentum and energy conservation laws

$$\partial_t \rho + \partial_x(\rho u) = 0, \tag{1.1}$$

$$\partial_t(\rho u) + \partial_x(\rho u^2 + p) = 0, \tag{1.2}$$

$$\partial_t(\rho E) + \partial_x((\rho E + p)u) = 0. \tag{1.3}$$

In the case of a one-fluid flow, the pressure would be a function of the density and the internal energy

$$p = p(\rho, e).$$

Because we consider two-fluid flows, our pressure is a function of the density and the internal energy but also of a supplementary unknown φ, the colour function

$$p = p(\rho, e, \varphi). \tag{1.4}$$

The colour function is transported with the flow

$$\partial_t \varphi + u \partial_x \varphi = 0.$$

Combining this transport equation with the mass conservation law (1.1) gives a conservative form of the colour function equation

$$\partial_t(\rho\varphi) + \partial_x(\rho\varphi u) = 0. \tag{1.5}$$

Finally, defining the conservative variables vector

$$W = (\rho, \rho u, \rho E, \rho\varphi)^T,$$

and the flux vector

$$F(W) = (\rho u, \rho u^2 + p, (\rho E + p)u, \rho\varphi u)^T,$$

the system (1.1)-(1.3), (1.5), (1.4) can be written

$$\partial_t W + \partial_x F(W) = 0.$$

For practical computations, we will use the pressure law of a mixture a stiffened gas. We consider a gas and a liquid satisfying stiffened gas laws

$$p = (\gamma_i - 1)\rho e - \gamma_i \pi_i,$$

with $i = 1$ for the gas and $i = 2$ for the liquid. The parameters $\gamma_i > 1$ and π_i are obtained from physical measurements. The mixture pressure is defined by

$$p(\rho, e, \varphi) = (\gamma(\varphi) - 1)\rho e - \gamma(\varphi)\pi(\varphi). \tag{1.6}$$

The mixture parameters are given by

$$\begin{aligned} \frac{1}{\gamma(\varphi) - 1} &= \varphi \frac{1}{\gamma_2 - 1} + (1 - \varphi)\frac{1}{\gamma_1 - 1}, \\ \frac{\gamma(\varphi)\pi(\varphi)}{\gamma(\varphi) - 1} &= \varphi \frac{\gamma_2 \pi_2}{\gamma_2 - 1} + (1 - \varphi)\frac{\gamma_1 \pi_1}{\gamma_1 - 1}, \end{aligned}$$

in such a way that $\varphi = 1$ in the pure liquid phase and $\varphi = 0$ in the pure gas phase. This system has nice mathematical properties: it is hyperbolic and the Riemann problem has a unique solution, even with large data [BHR03].

On the numerical side, the situation is more complicated. For instance it is now well-known that standard conservative finite volume schemes have a poor precision when applied to this kind of flow. Even worse, in some configurations of liquid-gas flows, the explicit Godunov cannot be used because it leads to negative densities.

2. The Lagrange-projection approach

For the finite volume approximation, we consider a sequence of times t_n, $n \in \mathbb{N}$, such that $t_0 = 0$ and $\tau_n = t_{n+1} - t_n > 0$. We also consider mesh points $x^n_{i+1/2}$ at time n. The cell C^n_i is the interval $]x^n_{i-1/2}, x^n_{i+1/2}[$. We denote by x^n_i the center of cell C^n_i

$$x^n_i = \frac{x^n_{i-1/2} + x^n_{i+1/2}}{2}.$$

The length of cell C^n_i is noted $h^n_i = x^n_{i+1/2} - x^n_{i-1/2}$. According to the notations, the mesh is moving but at some time step we will go back to the initial mesh at $n = 0$. We note

$$x_i = x^0_i, \quad C_i = C^0_i, \quad h_i = h^0_i, \quad etc.$$

We are looking for an approximation of W in the cell C^n_i

$$W^n_i \simeq W(x,t), \quad x \in C^n_i, \quad t \in]t_n, t_{n+1}[.$$

For the numerical resolution, we need an (exact or approximate) Riemann solver. The (exact or approximate) solution of the Riemann problem

$$\begin{aligned} \partial_t V + \partial_x F(V) &= 0, \\ V(x,0) &= \begin{cases} W_L \text{ if } x < 0, \\ W_R \text{ if } x > 0, \end{cases} \end{aligned}$$

is noted

$$R(\frac{x}{t}, W_L, W_R) = V(x,t).$$

Each time step of the Lagrange-projection scheme is made of two stages. In the first stage, we approximate the solution with a Lagrange scheme

$$h^{n+1/2}_i W^{n+1/2}_i - h^n_i W^n_i + \tau_n \left(F^n_{i+1/2} - F^n_{i-1/2} \right) = 0.$$

The Lagrange flux is defined by

$$\begin{aligned} F^n_{i+1/2} &= F(W^n_{i+1/2}) - u^n_{i+1/2} W^n_{i+1/2}, \\ W^n_{i+1/2} &= R(u^n_{i+1/2}, W^n_i, W^n_{i+1}), \end{aligned}$$

where the cell boundary $x^n_{i+1/2}$ moves at the velocity $u^n_{i+1/2}$ of the contact discontinuity in the resolution of the Riemann problem between $W_L = W^n_i$ and $W_R = W^n_{i+1}$

$$x^{n+1/2}_{i+1/2} = x^n_{i+1/2} + \tau_n u^n_{i+1/2}.$$

In particular, this defines the new size of cell C^n_i

$$h^{n+1/2}_i = x^{n+1/2}_{i+1/2} - x^{n+1/2}_{i-1/2} = h^n_i + \tau_n (u^n_{i+1/2} - u^n_{i-1/2}).$$

This formula is important because it can be generalized to higher dimensions. It permits to avoid the actual computation of the moved mesh.

After the Lagrange stage, we have to go back to the initial Euler mesh. This can be done with several methods

2.1. **The averaging projection.** In this approach, we average back on the Euler grid, with a simple L^2 projection

$$\begin{aligned} W_i^{n+1} &= \frac{\tau_n}{h_i}\max(u_{i-1/2}^n,0)W_{i-1}^{n+1/2} - \frac{\tau_n}{h_i}\min(u_{i+1/2}^n,0)W_{i+1}^{n+1/2} \\ &+ \left(1 - \frac{\tau_n}{h_i}\max(u_{i-1/2}^n,0) + \frac{\tau_n}{h_i}\min(u_{i+1/2}^n,0)\right) W_i^{n+1/2}. \end{aligned} \tag{2.1}$$

And we go back to the initial Euler grid

$$C_i^{n+1} = C_i, \quad h_i^{n+1} = h_i^n.$$

It can also be written

$$\begin{aligned} W_i^{n+1} = W_i^{n+1/2} - \frac{\tau_n}{h_i}\Big(&\max(u_{i-1/2}^n,0)(W_i^{n+1/2} - W_{i-1}^{n+1/2}) + \\ &\min(u_{i+1/2}^{n+1/2},0)(W_{i+1}^{n+1/2} - W_i^{n+1/2})\Big). \end{aligned} \tag{2.2}$$

In this way, it is clear that the projection step is an upwind approximation of

$$\partial_t W + u\partial_x W = 0.$$

This method is fully conservative and thus has a bad precision for multifluid problems [BHR03]. It is possible to improve the precision by the Saurel-Abgrall approach. It consists in performing a non-conservative projection on the colour function. Instead of projecting $\rho\varphi$ as in (2.1) we project directly φ, which gives

$$\begin{aligned} \varphi_i^{n+1} = \varphi_i^{n+1/2} - \frac{\tau_n}{h_i}\Big(&\max(u_{i-1/2}^n,0)(\varphi_i^{n+1/2} - \varphi_{i-1}^{n+1/2}) + \\ &\min(u_{i+1/2}^{n+1/2},0)(\varphi_{i+1}^{n+1/2} - \varphi_i^{n+1/2})\Big). \end{aligned}$$

This approach results in a globally non-conservative scheme: it induces a numerical mass transfer between the two phases. In the case of the stiffened gas pressure law (1.6) it can be proved that the resulting scheme preserves constant (u,p) states.

2.2. **The Glimm projection.** In this approach, we construct a sequence of random or pseudo-random numbers $\omega_n \in [0,1]$. According to this number we take

$$\begin{aligned} W_i^{n+1} &= W_{i-1}^{n+1/2} \text{ if } \omega_n < \frac{\tau_n}{h_i}\max(u_{i-1/2}^n,0), \\ W_i^{n+1} &= W_{i+1}^{n+1/2} \text{ if } \omega_n > 1 + \frac{\tau_n}{h_i}\min(u_{i+1/2}^n,0), \\ W_i^n &= W_i^{n+1/2} \text{ if } \frac{\tau_n}{h_i}\max(u_{i-1/2}^n,0) \le \omega_n \le 1 + \frac{\tau_n}{h_i}\min(u_{i+1/2}^n,0). \end{aligned} \tag{2.3}$$

And we go back to the initial Euler grid

$$h_i^{n+1} = h_i^n.$$

This method is only statistically conservative [Gl65]. It preserves exactly constant velocity-pressure states. The contacts are solved in one point. The drawback is that the solution may be noisy. In particular, for strong shocks the whole method does not converge towards the correct entropy solution.

A good choice for the pseudo-random sequence ω_n is the (k_1,k_2) van der Corput sequence, computed by the following C algorithm

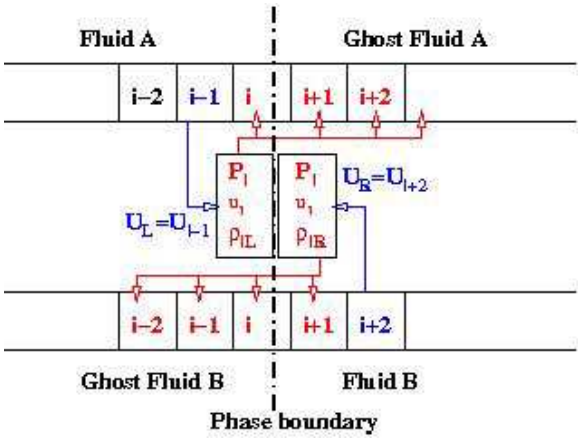

FIGURE 3.1. Sketch of the computation of the real and ghost fluid states from the interfacial states u_I, p_I and ρ_{IL}, ρ_{IR} determined by solving a two-phase Riemann problem for the states u_L and u_R.

```
float corput(int n,int k1,int k2){
  float corput=0;
  float s=1;
  while(n>0){
    s/=k1;
    corput+=(k2*n%k1)%k1*s;
    n/=k1;
  }
  return corput;
}
```

In this algorithm, k_1 and k_2 are two relatively prime numbers and $k_1 > k_2 > 0$. For more details, we refer to [Tor99]. In practice, we consider the $(5, 3)$ van der Corput sequence.

2.3. **Mixed projection.** In order to improve the convergence of the Glimm approach, it is possible to follow the following mixed projection step. If cell C_i and its two neighbours are in the same fluid, i.e. if

$$(\varphi_{i-1}^n - \frac{1}{2})(\varphi_i^n - \frac{1}{2}) > 0 \text{ and } (\varphi_i^n - \frac{1}{2})(\varphi_{i+1}^n - \frac{1}{2}) > 0,$$

then, we follow the projection given by (2.2). In all the other cases, we follow the Glimm projection (2.3). This approach allows a better precision at the interface because it is resolved in only one point.

3. THE MODIFIED GHOST FLUID APPROACH

The real Ghost Fluid method, developed by Wang, Liu and Khoo in 2006 [WLK06] is an adaptation of the original ghost fluid method of Fedkiw.

In this method, the interface between the liquid and the gas is located by a function ψ. In the liquid, we have $\psi > 0$ and in the gas, $\psi < 0$. And thus,

the interface corresponds to the level-set $\psi = 0$. As in the previous method, the level-set function ψ is transported in the flow

$$\partial_t \psi + u \partial_x \psi = 0. \tag{3.1}$$

And we switch from the pressure law of the liquid to the pressure law of the gas according to the sign of ψ. It is clear that the differences between the color function model and the level-set model are only formal. However, the numerical implementations are rather different.

The level-set function ψ is approximated in cell C_i at time t_n by ψ_i^n. The solution is approximated by a Godunov scheme

$$W_i^{n+1} = W_i^n - \frac{\tau_n}{h_i}\left(F_{i+1/2}^{n,-} - F_{i-1/2}^{n,+}\right), \tag{3.2}$$

with a possible non-conservative flux $F_{i+1/2}^{n,-} \neq F_{i+1/2}^{n,+}$. If the two cells C_i and C_{i+1} are filled with the same phase, which is true if

$$\psi_i^n \cdot \psi_{i+1}^n > 0.$$

Then, we take the classical conservative Godunov flux

$$F_{i+1/2}^{n,-} = F_{i+1/2}^{n,+} = F_{i+1/2}^n = F(R(0, W_i^n, W_{i+1}^n)).$$

If the phase boundary is lying between cell i and cell $i+1$ where cell i corresponds to fluid A and cell $i+1$ to fluid B, then it means that

$$\psi_i^n \cdot \psi_{i+1}^n < 0.$$

then the left and right state are taken from cells $i-1$ and $i+2$, respectively, to ensure access to states of the pure phases

$$W_L = W_{i-1}^n, \quad W_R = W_{i+2}^n.$$

We solve the Riemann problem between W_L and W_R. Let u_I be the contact velocity in this exact solution. We can define interfacial states to the left and to the right of the contact wave by

$$W_{IL} = \lim_{\xi \to u_I^-} R(\xi, W_L, W_R), \quad W_{IR} = \lim_{\xi \to u_I^+} R(\xi, W_L, W_R).$$

We have thus access to interfacial states for densities ρ_{IL}, ρ_{IR}, pressure p_I and velocity u_I left and right to the phase boundary. For fluid A, the state (ρ_{IL}, u_I, p_I) replaces the states of the cell i and defines the ghost states. The fluxes are thus

$$F_{i+1/2}^- = F(R(0, W_{IL}, W_{IL})), \quad F_{i+1/2}^+ = F(R(0, W_{IR}, W_{IR})).$$

The evolution equation is also slightly modified by

$$W_i^{n+1} = W_{IL} - \frac{\tau_n}{h_i}\left(F_{i+1/2}^{n,-} - F_{i-1/2}^{n,+}\right),$$

and

$$W_{i+1}^{n+1} = W_{IR} - \frac{\tau_n}{h_{i+1}}\left(F_{i+3/2}^{n,-} - F_{i+1/2}^{n,+}\right),$$

This procedure is sketched in Fig. 3. As a consequence, only single-phase Riemann problems are solved for each cell interface of fluid A to provide the numerical fluxes with the ghost cells as boundary conditions at the phase boundary. Then the same procedure is used for fluid B.

Thus near the phase boundary, two fluxes $\mathbf{F}_{i+\frac{1}{2}}^{n,\pm}$, one for each fluid, are defined. Away from the phase boundary, where only one numerical flux is computed at a

cell interface, the spatial order is improved by using a second-order reconstruction of the primitive variables ρ, u, p. The solution is advanced to the next time step by the finite volume scheme (3.2).

On the other hand, the level set function has also to be advanced. This is done first by solving numerically (3.1) with a standard upwind non-conservative finite volume scheme

$$\psi_i^{n+1,-} = \psi_i^n - \frac{\tau_n}{h_i}\left(\max(u_{i-1/2}^n,0)(\psi_i^n-\psi_{i-1}^n) + \min(u_{i+1/2}^n,0)(\psi_{i+1}^n-\psi_i^n)\right)$$

Periodically, the level-set function approximation is reinitialized in such a way that it remains a signed distance to the interface. This is formally obtained through the numerical resolution of an Hamilton-Jacobi equation

$$\begin{aligned}
\partial_\tau\widetilde{\psi}(x,\tau) + a(\widetilde{\psi})\partial_x\widetilde{\psi} &= S(\widetilde{\psi}),\\
a(\widetilde{\psi}) &= S(\widetilde{\psi})\frac{\partial_x\widetilde{\psi}}{\left|\partial_x\widetilde{\psi}\right|},\\
S(\widetilde{\psi}) &= \begin{cases} -1 & \text{if} \quad \widetilde{\psi}<0,\\ 0 & \text{if} \quad \widetilde{\psi}=0,\\ 1 & \text{if} \quad \widetilde{\psi}>0,\end{cases}\\
\widetilde{\psi}(x,\tau=0) &= \psi_i^{n+1,-}, \quad x\in C_i.
\end{aligned}$$

The level-set function is replaced by the reinitialized level-set function, *i.e.* we take

$$\psi_i^{n+1} = \widetilde{\psi}(x,\tau=\infty), \quad x\in C_i.$$

This procedure is described in more details in [MBKKH09].

Finally, during the update of the level set function, a cell may switch from one fluid to the other. This situation corresponds to a change of the sign between time step$n$ and time $n+1$, *i.e.* when $\psi_i^n\cdot\psi_i^{n+1}<0$. In this case, it is necessary to also update W_i^{n+1} on the corresponding cell. The fluid variables are recalculated using the equation of state of the new fluid. The cell being very close to the phase boundary, the velocities and the pressure, which are constant for both fluids at the phase boundary, are preserved. This modification was suggested by Barberon[**?**]. In addition to this approach, we propose the modification of the density. As no exact value for the density is known, the density is replaced by the density of the corresponding ghost cell. More precisely, if $\psi_i^n\cdot\psi_i^{n+1}<0$, and if $\psi_i^n\cdot\psi_{i+1}^n<0$, then, before computing the next time-step, we substitute the density by

$$\rho_i^{n+1} \leftarrow \rho_{IR}$$

and the energy e_i^{n+1} is also modified in such a way that

$$p_i^{n+1} = p(\rho_i^{n+1}, e_i^{n+1}, \psi_i^{n+1})$$

is not changed. This construction implies that the whole resulting scheme will preserve constant (u,p) states. On the other hand, it is also clear that the scheme is not conservative. For instance, the last update implies a mass and an energy transfer between the two fluids.

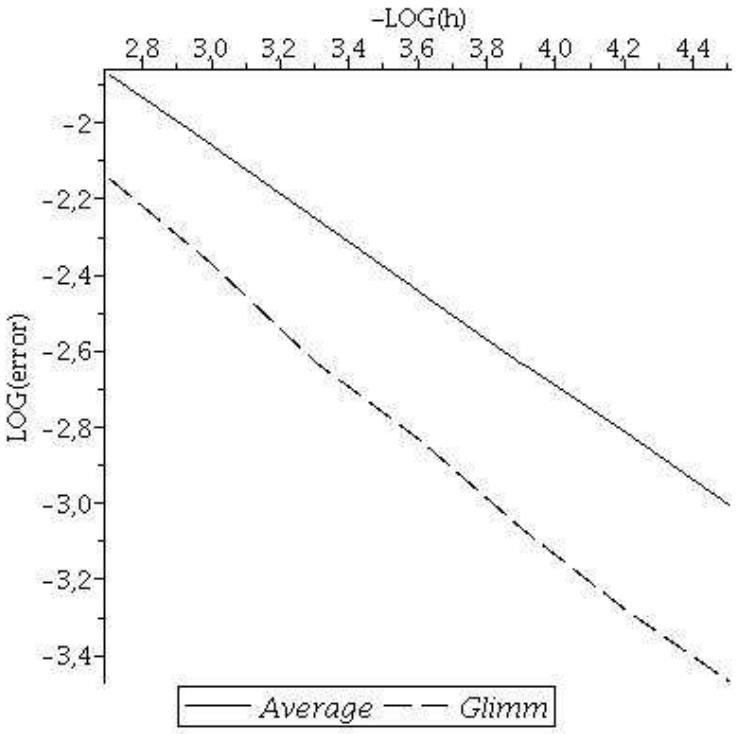

FIGURE 4.1. Convergence study: Glimm projection versus averaging projection, academic validation.

4. Numerical results

4.1. **Academic validation.** The first test consists in a two-fluid shock tube. The stiffened gas parameter are

$$\gamma_2 = 2, \quad \pi_2 = 1,$$
$$\gamma_1 = 1.4, \quad \pi_1 = 0.$$

We take for the left and right initial data

$$(\rho_L, u_L, p_L, \varphi_L) = (2, 1/2, 2, 1),$$
$$(\rho_R, u_R, p_R, \varphi_R) = (1, 1/2, 1, 0).$$

For the Lagrange-projection approach, the non-conservative projection and the Glimm projection are compared. We observe numerical convergence in the L^1 norm for the two methods and that the Glimm projection is more precise than the averaging projection. See Figure 4.1. The convergence rate for the two methods is approximately 0.6.

4.2. **1D academic shock-interface interaction.** An interface between two fluids is located a time $t = 0$ at position $x = 1$. The two fluids are moving to the left at the velocity $v = -1$. The fluid (2) is on the left, while the fluid (1) is on the right. A shock is arriving from the left at velocity $\sigma = 4$. The initial position of

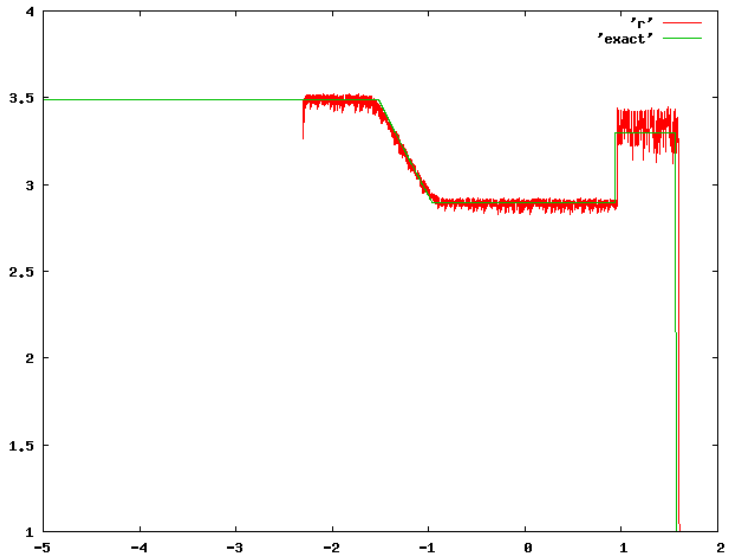

FIGURE 4.2. Glimm approach, density plot. BV explosion due to wall-heating effect propagation.

the contact and the shock are chosen in such way that they will meet together at the abscissa $x = 0$ at time $t = 1$. The EOS parameters are the following

$$\gamma_1 = 1.4 \quad \pi_1 = 0,$$
$$\gamma_2 = 2 \quad \pi_2 = 7.$$

The initial data are, if $x < -4$

$$(\rho_L, u_L, p_L, \varphi_L) = (3.4884, 1.1333, 23.333, 1),$$

if $x > 1$

$$(\rho_R, u_R, p_R, \varphi_R) = (1, -1, 2, 0),$$

and if $-4 \leq x \leq 1$

$$(\rho_M, u_M, p_M, \varphi_M) = (2, -1, 2, 1).$$

After that the shock and the contact waves have met at time $t = 1$, the solution is simply given by the resolution of a two-fluid Riemann problem between states (L) and (R). The solutions is sketched in Figure 4.5. The numerical data are recalled in Table 1.

4.2.1. *Lagrange plus projection schemes.* In this case, we observe that the Glimm approach does not converge. This behavior depends on the strength of the shock wave. A typical plot is given on Figure 4.2, where we compare the exact and the approximated densities at time $t = 1.5$.

In this case, we thus compare the averaging projection approach with the mixed projection approach. We obtained the results of Figure 4.3 The mixed projection has a better precision than the averaging projection.

We also provide on Figure 4.4 a comparison of the mixed and averaging projection schemes for the densities for a mesh of 500 cells of the interval $[-5; 2]$. The CFL

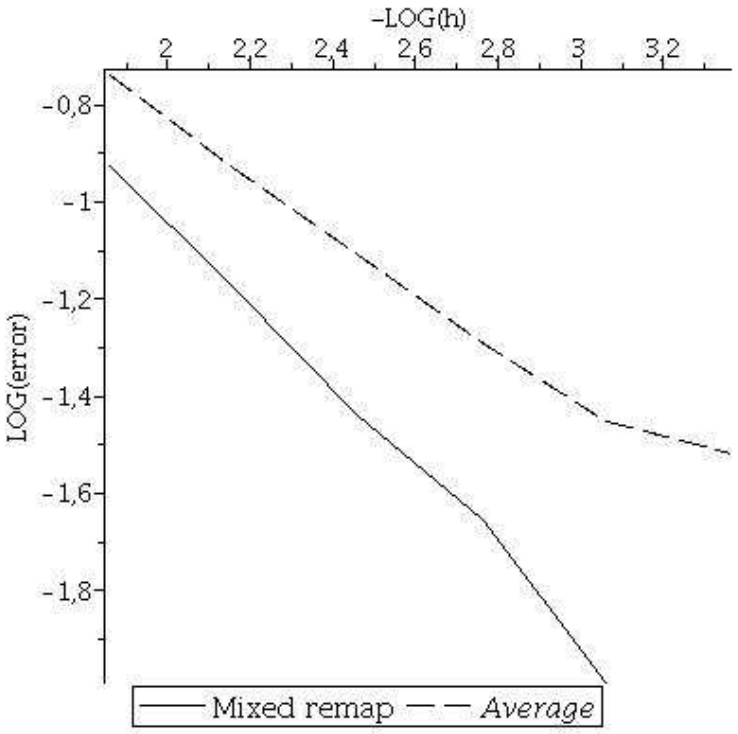

FIGURE 4.3. Academic shock-interface interaction. Convergence study. Mixed projection and averaging projection.

number is fixed to 0.7. It is interesting to observe that the interface position is very well resolved (in only one mesh point) by the mixed projection scheme and that this good resolution of the contact wave also implies an improvement of the precision in the left rarefaction wave.

4.2.2. *Modified Ghost fluid approach.* In order to compare the non-conservative methods of Saurel-Abgrall and the RGFM, several numerical solutions are compared with the exact solution and a convergence study is performed. The coarse discretization consists of 100 cells on which the multiscale-based transformation is applied [MBKKH09]. The convergence study is performed for grids having from 5 to 13 refinement levels L, i.e the uniform grid on the finest level consists of $2^L * 100$ cells. The threshold value in the grid adaptation is chosen as $\varepsilon = 10^{-5}$. This small value is chosen in such a way that the regions containing the finest grid cells are large enough to avoid additional error from larger cells. The errors obtained with the multiscale grid adaptation are thus comparable with those obtain with a uniform grid. Tests are performed with a CFL number of 0.9. Summary:Ω=[-5;2]m, $t \in$[0;1.5]s $N_0 = 100$, $5 \leq L \leq 13$, ϵ_L=1.e-5, CFL=0.9

In figures 4.6 and 4.7 are shown the comparison of the density for the two approaches with the exact solution, the dashed line, at $t = 1.5$ ms. The first figure corresponds to a grid with seven refinement levels and the second one to a very fine grid with twelve refinement levels. The global result is pictured in the middle and

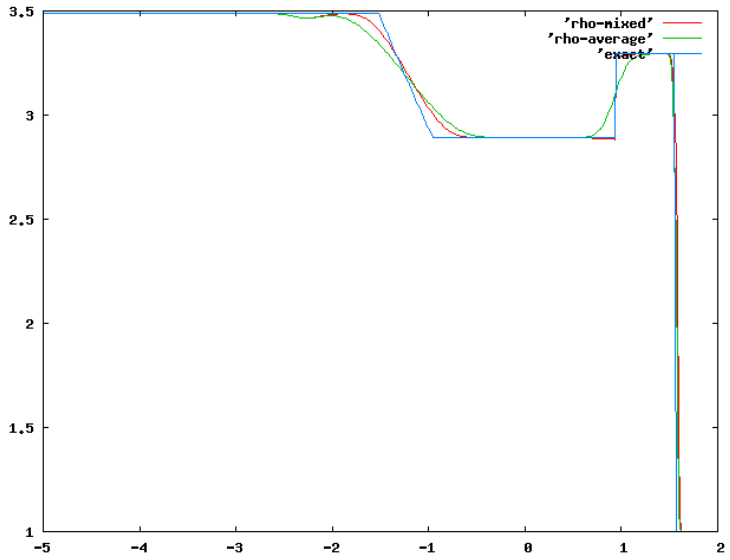

FIGURE 4.4. Density. Comparison of the mixed and averaging projection schemes.

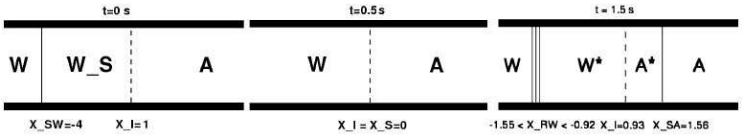

FIGURE 4.5. Initialization of the air-air shock-contact interaction

	U_W	U_{WS}	U_{W*}	U_{A*}	U_A
ρ [kg/m^3]	3.488	2	2.89415	3.2953	1
v [m/s]	1.13	-1	1.87672		-1
p [Pa]	23.33	2	13.88	13.88	2

TABLE 1. Air-Air shock-contact interaction.

a zoom of the shock position on the bottom left, a zoom of the plateau between the rarefaction wave and the contact on the top left and a zoom very close to the contact position on the right. In the last one, cell centers are marked by diamonds for the numerical results.

The Saurel-Abgrall approach generates oscillations at the bottom of the rarefaction wave due to the interaction between the shock and the contact. This is not the case for the RGFM that coincides quite well with the exact solution. With five more grid refinement levels, shown in picture 4.7, the amplitude of the oscillations largely reduce.

At the contact, there is a smearing of the density for the Saurel-Abgrall approach. This is easy to see in the zoom on the right in which the density for this approach decreases slowly instead of presenting a jump with the RGFM method. Due to the

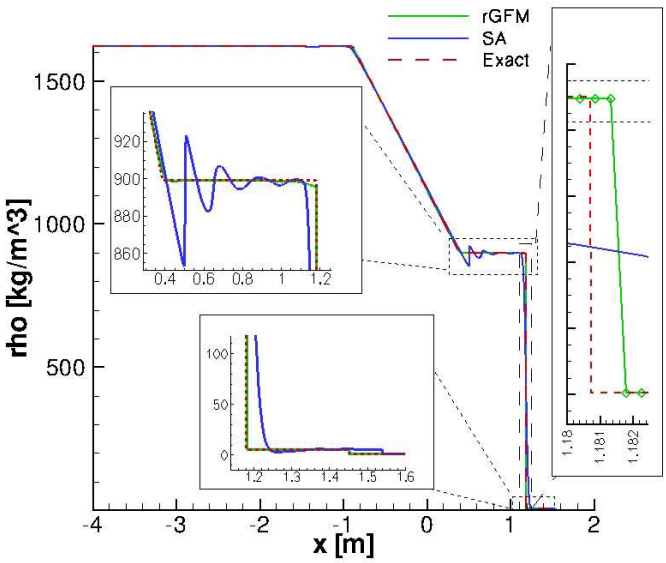

FIGURE 4.6. Results of the shock-contact interaction for 7 refinement levels at t=1.5 ms

construction of the ghost fluid method, we obtain the desired jump at the contact but this jump is a little bit shifted compared with the exact solution. As the cell centers are represented by diamonds on the pictures, for 7 refinement levels, we can see a shift in the position of the contact of 2 cells and in the computation with twelve levels of refinement, the shift is about 4 cells. This is summarized in Table 3.

Concerning the position of the shock, which is only visible in the zoom because of the big jump of density, we remark that its position is well predicted with the RGFM method for both computations. That is not really the case for the Saurel-Abgrall approach. Under grid refinement, the shift reduces as much as the smearing region at the contact.

Concerning the Saurel-Abgrall approach, the oscillations and the error in the position of the shock is only due to the previous shock-contact interaction. When only the Riemann problem is computed, i.e. when the computation starts at $t = 0.5$ ms, we obtain the results of Figure 4.9. In this simplified situation, the results are in good agreement everywhere with the exact solution. A comparison (shock-contact interaction and direct resolution of the Riemann problem) is shown in figure 4.8.

The L^1 error of the density are given in Table 2. The order of convergence for the Saurel-Abgrall approach is approximately 0.5. Concerning the RGFM, the error seems to tend to the same order under grid refinement.

4.3. **Air-water test case.** For the RGFM, we propose an additional test case consisting in a shock wave of Mach number 0.67 at the position $x = -3$ m running in the liquid that interacts with the air at $t = 0.5$ms at the position $x = 0$ m. The water ahead of the shock and the air are moving towards the shock at the velocity of 100 m/s. The computational domain is $[-4; 2]$m. The test is sketched in Figure

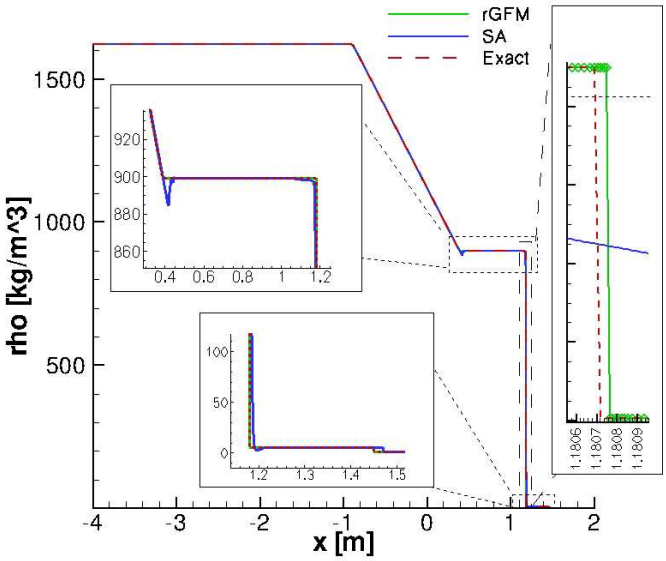

FIGURE 4.7. Results of the shock-contact for 12 refinement levels at t=1.5 ms

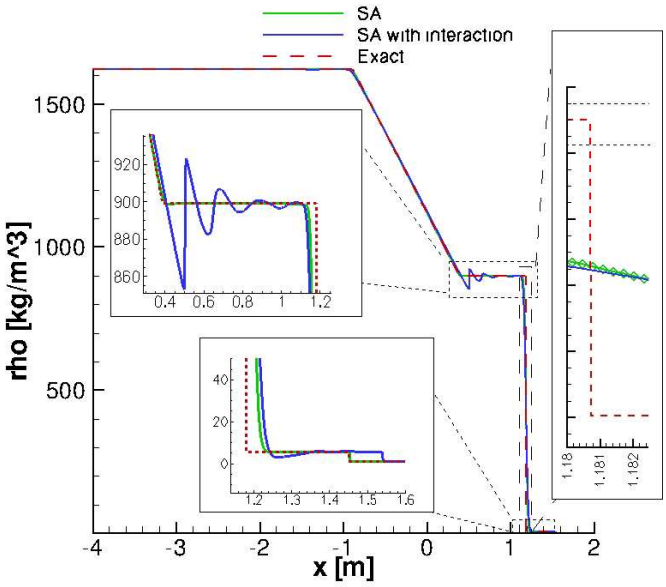

FIGURE 4.8. Results for 7 refinement levels at t=1.5 ms

4.9 and the different states are given in Table (4). The material parameters for the fluids are listed in Table 5.

	Saurel-Abgrall		RGFM	
Levels	L^1 error	Order	L^1 error	Order
5	10.20	-	1.8	-
7	4.81	0.54	0.51	0.91
8	3.27	0.56	0.31	0.72
9	2.24	0.54	0.17	0.87
10	1.55	0.53	0.11	0.67
11	1.09	0.51	6.90E-02	0.62
12	0.77	0.51	4.54E-02	0.60
13	0.54	0.5	3.05E-02	0.57

TABLE 2. Water-Air global L^1 error.

		Saurel-Abgrall		RGFM	
Levels	h_L [m]	Error	Order	Error	Order
5	1.87E-03	7.12E-03	-	3.55E-03	-
7	4.69E-04	3.51E-03	0.51	1.03E-03	0.89
8	2.34E-04	2.46E-03	0.51	5.25E-04	0.97
9	1.17E-04	1.72E-03	0.52	2.93E-04	0.84
10	5.86E-05	1.20E-03	0.52	1.59E-04	0.88
11	2.93E-05	8.42E-04	0.51	9.21E-05	0.79
12	1.46E-05	5.92E-04	0.51	5.43E-05	0.76
13	7.32E-06	4.22E-04	0.49	3.38E-05	0.68

TABLE 3. Water-Air error in the interface position where h_L is the grid size for L refinement levels.

	U_W	U_{WS}	U_{W*}	U_{A*}	U_A
ρ [kg/m^3]	1620.6	1000	900	5.57	1
v [m/s]	1087.1	-100	2361.4	2361.4	-100
p [Pa]	3.6801E+09	1E+05	7.48506E+06	7.48506E+06	1E+05

TABLE 4. Water-Air shock-contact interaction.

	γ [-]	π [Pa]
Water	3.0	7.499e+8
Air	1.4	0

TABLE 5. Material parameters for water and air.

5. Gas bubble oscillations

In this section we apply the random projection scheme to a bubble oscillations test case described in[HMM08, MBKKH09, Ma10]. Despite the quasi one-dimensional framework, the test case implies very long computations and very fine meshes. We compare with the results obtained with the RGFM on arbitrary refined grids.

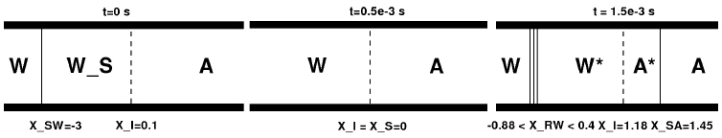

FIGURE 4.9. Initialization of the water-air shock-contact interaction

6. Conclusion

In this paper, we have proposed a new scheme for computing two-fluid flows. The pressure oscillations at the interface are avoided thanks to a Lagrange and projection approach. In the Lagrange step, the contact waves are perfectly resolved and the interface is not smeared. In the projection step, we employ a random sampling strategy. The resulting scheme preserves the constant velocity-pressure states and the interface is solved within one grid point.

The whole approach performs well for weak shocks. But in presence of strong shocks, it appears to be oscillating. Therefore, we had to adapt the projection step and only apply it at the two-fluid interface, which is located thanks to the jumps of the colour function. We proposed then numerical results that demonstrate the good convergence of the scheme, despite that it is not conservative. We surprisingly observed this convergence property for other non-conservative schemes for two-fluid flows.

Finally, we apply our scheme to a more challenging problem, which consists in the simulation of the oscillations of gas bubble in a compressible liquid. Our simple scheme gives good results, even if its precision is less than the more sophisticated RGFM coupled with arbitrary mesh refinement.

Our prospects are in several directions:

- first we would like to improve the precision of the random projection scheme. The first obvious way to do it is to couple it with a second order MUSCL extension. This extension has to be deactivated at the interface, in order to avoid oscillations. For the spherical bubble computations, another way to improve the precision is to modify the scheme in order that it becomes well-balanced. This can be done by adapting the method described in [HHM10].
- a challenging extension would consist in extending the random projection scheme to two- or three-dimensional computations. This could be tried for example by a simple directional splitting algorithm. This will be the object of a forthcoming work.

References

[Abg88] R. Abgrall. Generalisation of the roe scheme for the computation of mixture of perfect gases. Recherche Aérospatiale, 6:31–43, 1988.

[AK10] Rémi Abgrall, Smadar Karni. A comment on the computation of non-conservative products. Journal of Computational Physics 229 (2010) 2759–2763

[BHR03] T. Barberon, P. Helluy, and S. Rouy. Practical computation of axisymmetrical multifluid flows. International Journal of Finite Volumes, 1(1) :1–34, 2003.

[CC08] Chalons, C.; Coquel, F. Capturing infinitely sharp discrete shock profiles with the Godunov scheme. Hyperbolic problems: theory, numerics, applications, 363–370, Springer, Berlin, 2008.

[CG07] Chalons, Christophe; Goatin, Paola Transport-equilibrium schemes for computing contact discontinuities in traffic flow modeling. Commun. Math. Sci. 5 (2007), no. 3, 533–551.

[FAMO99] Fedkiw, Ronald P.; Aslam, Tariq; Merriman, Barry; Osher, Stanley A non-oscillatory Eulerian approach to interfaces in multimaterial flows (the ghost fluid method). J. Comput. Phys. 152 (1999), no. 2, 457–492.

[Gl65] Glimm, James Solutions in the large for nonlinear hyperbolic systems of equations. Comm. Pure Appl. Math. 18 1965 697–715.

[HHM10] P Helluy, J Herard, H Mathis. A well-balanced approximate Riemann solver for variable cross-section compressible flows. AIAA Proc. 22-25 Jun, 2009

[HMM08] Helluy, Philippe; Mathis, Hélène; Müller, Siegfried An ALE averaging approach for the computing of bubble oscillations. Finite volumes for complex applications V, 487–494, ISTE, London, 2008.

[HL94] Hou, Thomas Y.; LeFloch, Philippe G. Why nonconservative schemes converge to wrong solutions: error analysis. Math. Comp. 62 (1994), no. 206, 497–530.

[Kar94] Karni, Smadar Multicomponent flow calculations by a consistent primitive algorithm. J. Comput. Phys. 112 (1994), no. 1, 31–43.

[KL10] Kokh, S.; Lagoutière, F. An anti-diffusive numerical scheme for the simulation of interfaces between compressible fluids by means of a five-equation model. J. Comput. Phys. 229 (2010), no. 8, 2773–2809.

[Ma10] Mathis, H. Étude théorique et numérique des écoulements avec transition de phase. PhD thesis, Université de Strasbourg, 2010. http://tel.archives-ouvertes.fr/IRMA/tel-00516683/fr/

[MBKKH09] S. Müller, M. Bachmann, D. Kröninger, T. Kurz, P. Helluy. Comparison and validation of compressible flow simulations of laser-induced cavitation bubbles. Computers & Fluids. 38 (9):1850-1862, 2009.

[SA99a] Saurel, Richard; Abgrall, Rémi A simple method for compressible multifluid flows. SIAM J. Sci. Comput. 21 (1999), no. 3, 1115–1145

[SA99b] Saurel, Richard; Abgrall, Rémi A multiphase Godunov method for compressible multifluid and multiphase flows. J. Comput. Phys. 150 (1999), no. 2, 425–467.

[Tor99] Toro, Eleuterio F. Riemann solvers and numerical methods for fluid dynamics. A practical introduction. Second edition. Springer-Verlag, Berlin, 1999.

[WK05] Wackers, Jeroen; Koren, Barry A fully conservative model for compressible two-fluid flow. 8th ICFD Conference on Numerical Methods for Fluid Dynamics. Part 2. Internat. J. Numer. Methods Fluids 47 (2005), no. 10-11, 1337–1343

[WLK06] Wang, C. W. ; Liu, T. G. ; Khoo, B. C. A real ghost fluid method for the simulation of multimedium compressible flow. SIAM J. Sci. Comput. 28 (2006), no. 1, 278–302

RWTH Aachen and IRMA, Université de Strasbourg
E-mail address: helluy@math.unistra.fr